HHS Public Access

Author manuscript

Ultrasound Med Biol. Author manuscript; available in PMC 2017 February 01.

Published in final edited form as:

Ultrasound Med Biol. 2016 February ; 42(2): 481–492. doi:10.1016/j.ultrasmedbio.2015.10.009.

SAFETY VALIDATION OF REPEATED BLOOD–BRAIN BARRIER DISRUPTION USING FOCUSED ULTRASOUND

Thiele Kobus[*,†], **Natalia Vykhodtseva**[*], **Magdalini Pilatou**[*], **Yongzhi Zhang**[*], and **Nathan McDannold**[*]

[*]Department of Radiology, Brigham and Women's Hospital, Harvard Medical School, Boston, MA, USA [†]Department of Radiology and Nuclear Medicine, Radboud University Medical Center, Nijmegen, The Netherlands

Abstract

The purpose of this study was to investigate the effects on the brain of multiple sessions of blood–brain barrier (BBB) disruption using focused ultrasound (FUS) in combination with micro-bubbles over a range of acoustic exposure levels. Six weekly sessions of FUS, using acoustical pressures between 0.66 and 0.80 MPa, were performed under magnetic resonance guidance. The success and degree of BBB disruption was estimated by signal enhancement of post-contrast T1-weighted imaging of the treated area. Histopathological analysis was performed after the last treatment. The consequences of repeated BBB disruption varied from no indications of vascular damage to signs of micro-hemorrhages, macrophage infiltration, micro-scar formations and cystic cavities. The signal enhancement on the contrast-enhanced T1-weighted imaging had limited value for predicting small-vessel damage. T2-weighted imaging corresponded well with the effects on histopathology and could be used to study treatment effects over time. This study demonstrates that repeated BBB disruption by FUS can be performed with no or limited damage to the brain tissue.

Keywords

Focused ultrasound; Blood–brain barrier disruption; Multiple sessions; Safety study; Magnetic resonance guidance; Histologic evaluation

INTRODUCTION

The blood–brain barrier (BBB) is a functional and structural barrier that protects the brain. It regulates transport of molecules from the vasculature to the central nervous system (Abbott and Romero 1996). The BBB consists of endothelial cells connected by tight junctions, pericytes, a basement membrane and endfeet of astrocytes. Only small (molecular weight < 400 Da), hydrophobic molecules can pass the BBB. The BBB is a hurdle in the development of drugs effective in the central nervous system because practically all large-molecule drugs and more than 98% of small-molecule drugs do not pass the BBB (Pardridge 2003). Several

Address correspondence to: Thiele Kobus, 221 Longwood Avenue, Boston, MA 02115, USA. thiele.kobus@radboudumc.nl.

approaches have been proposed to circumvent this barrier (*e.g.,* Bobo et al. 1994; Doolittle et al. 2000; Guerin et al. 2004; Pardridge 2002a, 2002b), but these are either invasive or non-localized. In clinical practice, many therapeutic agents need to be administered multiple times over the course of several weeks or months to be effective. This means that the BBB needs to be disrupted repeatedly over an extended period of time. Therefore, a method that can non-invasively and reversibly disrupt the BBB at targeted locations would have major impact on clinical neuroscience.

A technique with this potential was introduced in 2001 (Hynynen et al. 2001). The researchers used focused ultrasound (FUS) in combination with micro-bubbles circulating in the vasculature to temporarily disrupt the BBB. In the ultrasound focal region, an interaction between the micro-bubbles, small gas bubbles usually used as ultrasound contrast agent, and ultrasound waves takes place. Pre-clinical studies have shown that these interactions cause a temporary disassembly of the tight junction proteins and stimulate active transport, making it possible to deliver drugs through the BBB (Fan et al. 2011; Hynynen et al. 2001; Shang et al. 2011; Sheikov et al. 2006, 2008; Xia et al. 2012). A few hours after the focused ultrasound therapy, the barrier is closed, and the brains appear normal in light microscopy (Baseri et al. 2010; Hynynen et al. 2005; Hynynen et al. 2006; McDannold et al. 2005).

When the BBB is disrupted by FUS in the presence of micro-bubbles, small vessel damage can occur, which can have minimal to severe consequences. These consequences can be studied with histologic examinations. Previously, the histologic effects of a single treatment of FUS in combination with micro-bubbles have been examined (Baseri et al. 2010; Hynynen et al. 2005, 2006; McDannold et al. 2005). These studies have shown only negligible effects on the tissue, largely related to the presence of microscopic regions containing extravasated erythrocytes, so-called petechiae. Histologic effects of multiple sonications were investigated in one non-human primate, but were not studied systematically (McDannold et al. 2012). The cumulative histologic effects of repeated stress to the brain vasculature are unknown.

In this study, the effects of repeatedly disrupting the BBB were studied. By performing the sonications under magnetic resonance (MR) guidance, the ultrasound focus could be targeted at the same brain regions during six weekly treatments. Furthermore, MR imaging (MRI) was used to determine the success of each treatment and obtain information about the effects of the treatment over time, although at a relatively low spatial resolution. Histologic analysis was performed for each animal after the last session. MRI and histopathology provided complementary information about the effects of repeated BBB disruptions. The results of these experiments will be important to move this technology to the clinic and to aid in evaluating the potential risks and benefits for different therapeutic applications.

MATERIALS AND METHODS

Animals

The study was approved by the Institutional Animal Care Committee. Fifteen healthy Sprague-Dawley rats (Charles River Laboratories, Boston, MA) were included in this study. The animals were divided in three groups. Each group received six weekly ultrasound

treatments at a different set of pressure amplitudes. The weight of the animals was measured each week. The animal weight at the start of the sonications was 325 ± 12 g for group 1 (lowest pressure group), 276 ± 63 g for group 2 and 197 ± 83 g for group 3 (highest pressure group). The animals were sacrificed between 1 h and 36 h after the last sonication.

MR-guided ultrasound procedures

Setup—The setup for the sonications is shown in Figure 1. A single-element, spherically-focused transducer (diameter =10 cm, f-number =0.8, frequency =690 kHz) was used to generate the ultrasound field. The half-maximum pressure amplitude width and length of the focal region were 2.3 and 14 mm, respectively (Hynynen et al. 2005). The transducer was mounted to a three-axis positioning system, placed in a tank with degassed water and connected to a matching circuit. To generate the ultrasound signal, an arbitrary waveform generator (Model 395, Wavetek Inc., San Diego, CA) and an RF amplifier (Model 240 L, ENI Inc., Rochester, NY) were used. The electrical power was monitored with a power meter (Model E4419 B, Agilent, Santa Clara, CA) and a dual-directional coupler (Model C594810-C, Werlatone, Patterson, NY).

Animal preparation—The animals were anesthetized with a mix of 80 mg/kg ketamine (Aveco Co., Inc., Fort Dodge, IA) and 10 mg/kg of xylazine (Lloyd Laboratories, Shenandoah, IA) *via* intra-peritoneal injection. The hair on the animal's head was removed and a catheter was inserted into the tail vein. The rat was placed in supine position in the sonication system (Fig. 1).

MRI guidance—The sonications were performed in a clinical 3 T MRI system (Signa, GE Healthcare, Milwaukee, WI). After placement of the animal, fast gradient echo images were obtained to localize the brain. Next, axial presonication T1-weighted imaging (T1-WI) and, in most sessions, axial T2-weighted imaging (T2-WI) were obtained with a fast spin echo sequence. The image parameters are provided in Table 1. T1-WI in combination with a gadolinium-based MRI contrast agent is commonly used to confirm BBB disruption. The intact BBB does not allow these agents to extravasate from the capillaries. A hyper-intense region on post-contrast T1-weighted images indicates extravasation of gadolinium and thus successful BBB disruption. Therefore, after the sonications, a bolus of 0.25 mL/kg MRI contrast agent gadopentetate dimeglumine (Gd-DTPA, molecular weight 938 Da; Magnevist, Bayer HealthCare Pharmaceuticals Inc., Wayne, NJ) was injected and T1-WI was repeated to confirm BBB disruption. This was followed by T2-WI.

Sonications—After registration of the ultrasound focal point to the MRI system coordinates, pre-sonication MR-images were used to select the targets for sonication. The ultrasound contrast agent Definity (Lantheus Medical Imaging, North Billerica, MA) was injected before each sonication at a dose of 10 μL/kg, which is the clinically recommended dose for ultrasound imaging. For the injections, Definity was diluted 10 times with phosphate-buffered saline. Immediately after IV injection of Definity, 10-ms burst sonications were applied for 60 s at a frequency of 1 Hz. The ultrasound contrast agent was immediately flushed with saline. A delay of at least 2 min between sonications was used, so that most micro-bubbles were cleared from the vasculature before the next IV injection.

Three spots, 1 mm apart, in the right hemisphere were sonicated to mimic a clinical treatment. Acoustic powers of 0.24, 0.32 and 0.40 W were used. These power levels corresponded with peak negative pressure amplitudes in water of 0.66, 0.73 and 0.80 MPa. Table 2 gives the used pressure per week for each animal. Successful BBB disruption was confirmed with contrast-enhanced T1-WI. O'Reilly et al. (2011) observed that pressure attenuation through the skull bone was proportional to the weight of the animals at sub-megahertz frequencies, which has been attributed to overall animal growth, including thickening of the skull bone. For the animals sonicated at the lowest exposure levels, the acoustic power was increased starting at week 4 to ensure successful BBB disruption, as the rats grew and gained weight every week.

Histology

Between 1 h and 36 h after the last session (Table 2), the animals were deeply anesthetized with ketamine and xylazine and euthanized by transcardial perfusion of 100 mL 0.9% NaCl, followed by 250 mL 10% buffered formalin phosphate to fix the brain. Each brain was embedded in paraffin and serially cut in 5-μm axial sections. Per animal, six sections, 250 μm apart, were stained with hematoxylin and eosin (H&E). Furthermore, one section was stained for glial fibrillary acidic protein (GFAP) to study the activated astrocyte cells. In one brain, where possible mineralization sites were found on the H&E section, a Von Kossa staining was used to confirm mineralization.

Analysis of histology

Consequences of vascular damage as seen on H&E sections—FUS in combination with micro-bubbles may lead to small-vessel damage, which includes micro-hemorrhages if the vessel walls reach the point of rupture. The consequences of this small-vessel damage as expressed on H&E sections depend on the time between the impact and the sacrifice of the animal. Fresh micro-hemorrhages (for example, from the last FUS session) are recognizable on H&E sections by extravasated erythrocytes. Older hemorrhages are signified by hemosiderin particles, which are the result of phagocytosis of the hemoglobin and erythrocytes by the macrophages. Local inflammation can be involved, seen on H&E sections as macrophage infiltrations. Occlusion of small vessels and hemorrhages can also result in focal and acute ischemia and tissue necrosis. Necrosis can selectively affect specific neurons (selective neuronal necrosis) or involve the complete tissue and progress to liquefactive necrosis. Eventually, affected regions can contain glial micro-scar formations, characterized by, among other aspects, astrogliosis and increased synthesis of GFAP. If the regular processes forming a glial scar are not strong enough to fill the tissue defects, cyst-like cavities can be formed. Other signs of the reparative process are mineralization spots (deposition of iron and calcium salts).

Analysis—An expert in animal brain histopathology inspected all stained sections. For each animal, the H&E sections with the most evident effects were selected. These and the sections stained with GFAP and Von Kossa were digitized with a Zeiss slide scanner (Oberkochen, Germany). The H&E sections were inspected for signs and consequences of vascular damage. Fresh micro-hemorrhages produced during the last (sixth) session were evaluated separately from the consequences of small-vessel damage produced during the

previous five sessions. The size of glial scars was measured. The GFAP sections were examined for activation of astroglial cells. The Von Kossa stained section was used to confirm the presence of mineralization.

Analysis of MRI

A region of interest (ROI) was drawn around the enhancing voxels on one of the post-contrast T1-weighted slices. Care was taken to exclude the ventricles from the ROI. On the contralateral hemisphere of the brain, the ROI at the same location and of the same size was drawn. The difference in signal intensity change in pre- and post-sonication T1-WI (ΔSI) was determined between the treated and contralateral brain regions. When more than one series of post-contrast T1-weighted images was obtained, the average enhancement was determined over multiple series. The size of the enhancing area was determined from the number of voxels in the ROI. The average and standard deviation of ΔSI and the size of the enhancing area (ROI-area) were determined for the three acoustic pressures and compared using ANOVA with a Tukey-Kramer post-test. Furthermore, the Pearson correlation coefficient between ΔSI and the ROI-area was determined, as was the Kendall's τ for the correlation between the acoustic pressure and ΔSI or the ROI-area.

Pre-sonication T1-weighted and post-sonication T2-weighted images—and, if acquired, pre-sonication T2-weighted images—were inspected for hypo- or hyper-intense regions. The findings of each week were compared. A distinction was made between permanent effects on T2-weighted images and temporary effects from the treatment. Finally, the results of the MRI analysis were related to the results of the histopathological analysis. Analyses were performed in Matlab (R2013 b, Math-works, Natick, MA) or GraphPad Prism (GraphPad Software, Inc., La Jolla, CA).

RESULTS

Contrast-enhanced T1-weighted MRI

Contrast-enhanced T1-WI is a common method to confirm BBB disruption. Signal enhancement on post-contrast T1-weighted images indicates extravasation of contrast, which does not extravasate from intact capillaries.

Eighty-nine of the 90 sessions led to successful BBB disruption as confirmed by signal enhancement on post-contrast T1-WI. One session at 0.73 MPa did not lead to BBB disruption. ΔSI could not be determined for all sessions: two animals moved between pre- and post-contrast images and exact repositioning could not be assured, and in five animals a data storage failure led to loss of the raw data of one or two sessions.

For animals sonicated at 0.66 MPa, the average ΔSI and standard deviation were 23.5% ± 17.8%, ranging from 5.4% to 54.5% (9 of 16 sessions analyzed; Fig. 2). The average ΔSI was 25.0% ± 12.7% (range: 3.7%–63.1%) in animals sonicated at an acoustic pressure of 0.73 MPa (44 of 46 sessions analyzed). For the animals sonicated at 0.80 MPa, the average ΔSI was 38.2% ± 28.7% (27 of 28 sessions analyzed). There was substantial inter- and intra-animal variability in ΔSI (Fig. 2). For example, the lowest ΔSI at 0.80 MPa was 7.8%, while the highest was 116.9%. ΔSI was significantly different between animals sonicated at 0.80

MPa and 0.73 MPa, but no significant difference in ΔSI was found at an acoustic pressure of 0.66 MPa. A small, but significant correlation existed between the acoustic pressures and ΔSI ($\tau = 0.19$, $p < 0.05$).

The average and standard deviation of the ROI area were 4.0 ± 1.8 mm^2, 4.8 ± 1.8 mm^2 and 5.6 ± 1.8 mm^2 for pressures of 0.66, 0.73 and 0.80 MPa, respectively. Although these were not significantly different from each other, a significant correlation was found between the acoustic pressures and ROI area ($\tau = 0.22$, $p < 0.05$). There was a significant Pearson correlation ($r = 0.32$, $p < 0.01$) between the ROI area and ΔSI.

The targeting accuracy was reasonable. In 5/15 animals, the same region was sonicated during all sessions. The center of the enhancing region was off by approximately 2–3 mm during one session in 6/15 animals. This was also the case in 3/15 animals during two sessions (2–3.5 mm) and in one animal during three sessions (4 mm maximum).

T2-weighted imaging

Changes observed on T2-WI provide information about acute and permanent alterations in the rat brain. An enhancement in signal intensity can indicate an increase in the water content, for example in case of a hemorrhage, edema or cyst. A hypo-intensity on T2-WI can indicate several changes, such as the presence of hemosiderin, calcium deposits, selective neuronal necrosis and gliosis.

T2-WI was acquired before sonication in 59 of 90 sessions (11/15 animals) and after sonication in all sessions. Fifty-two pre-sonication and 82 post-sonication T2-weighted images were analyzed; the other images could not be analyzed due to data storage failure or animal movement (awakening). In 59 of 82 post-sonication T2-weighted images, a light hyper-intensity in the sonicated area was observed. Except for 4/15 animals with a permanent hyper-intense spot on T2-WI, none of the other light hyper-intensities were seen on pre-sonication T2-weighted images the following week(s), which suggests that these light post-sonication hyper-intensities were temporary. The results of the qualitative analysis of T2-WI, excluding the light temporary hyper-intensities, are summarized in Table 3.

No abnormalities on the pre-sonication T2-WI caused by the sonications in earlier sessions were observed in 3/15 animals (Fig. 3b–c). In 12/15 animals, tissue changes were observed on T2-WI expressed as hypo-intense or hyper-intense areas, or as an enlarged ventricle at the sonicated site. A hypo-intense area was visible on pre- and/or post-sonication images for at least 2 consecutive wk in 7/15 animals (Fig. 4b–c). In 4/15 animals, a hyper-intensity was seen on pre-sonication T2-weighted images for 4–5 consecutive wk. Except for one animal, the size of this hyper-intensity decreased over the week and in one animal it was completely resolved on the images of the last session (Fig. 5b–d). Besides the hyper-intensity, hypo-intense spots were also present in 2/4 animals. In 3/15 animals, the lateral ventricle at the sonicated site was enlarged as a result of the sonications. In 2/3 animals, these enlarged ventricles appeared together with hypo- or hyper-intensities, but in one animal, this was the only permanent observable effect on T2-WI.

Pre-contrast T1-weighted imaging

The T1 relaxation time is long in cysts, like in the ventricles, resulting in a hypo-intense region on T1-WI. On the other hand, calcium deposits, selective neuronal necrosis and gliosis reduce the T1 relaxation time, which leads to hyper-intensities on T1-WI.

In 2/15 animals, a hypo-intense region on pre-contrast T1-WI was observed, which coincided with a hyper-intensity on T2-WI. A hyper-intense region was present on the pre-contrast T1-WI in 4/15 animals for at least 4 wk (Table 3). In five other animals, a very light temporarily hyper-intense region was observed on pre-contrast T1-WI for 1 wk and in another animal for 3 wk.

Histopathology

No tissue changes were produced during the last (sixth) session in 5/10 animals sonicated at an acoustic pressure of 0.73 MPa (Fig. 3). In the five other animals sonicated at the same acoustic pressure, scattered micro-hemorrhages (petechiae) were observed (Fig. 4g, Table 4). At an acoustic pressure of 0.80 MPa, hemorrhages were produced in 5/5 animals during the last session. In 3/5 animals, the micro-hemorrhages were associated with acute ischemic changes and resulted in selective neuronal necrosis (Fig. 6b–c). Of the other two animals, multiple hemorrhages were produced in one and a hemorrhagic infarct in the other.

Table 3 provides an overview of the consequences of vascular damage that were produced during one or more of the five previous sessions. In 2/15 animals, both sonicated at 0.66 and 0.73 MPa, no affected area or only a small area with macrophage infiltration was observed. In 10/15 animals, the sonications had resulted in a micro-scar formation (Fig. 3e and Fig. 4f). These scars were typically small (<0.5 mm). GFAP-immunolabeled sections in these areas contained astrocytes identified as being reactive based on their thick cytoskeletal processes (Fig. 3f). Besides the scars, one or more cyst-like cavities were formed in 4/15 animals (Fig. 5f). In 11/15 animals, individual or scattered hemosiderin particles were observed, signifying old hemorrhagic sites (Fig. 6d). Mineralization spots were observed in 5/15 animals (Fig. 7). In some animals, several separated areas with different histopathological features were found (Fig. 4). The most severe damage was found in 2/15 animals, sonicated at 0.8 MPa. In one of them, the affected region contained multi-focal deposits of minerals at the sites of former cell necrosis (Fig. 7). In the second animal, a large infarcted region with cyst and scar formations, scattered areas of mineralization and extensive hemorrhages were observed.

Histopathology and MRI

Vascular damage produced during the last (sixth) FUS session—Table 4 summarizes the MRI and histopathology results of the last (sixth) session. The average ΔSI of the sixth session for the five animals without micro-hemorrhages was 23.2% ± 16.1% (0.73 MPa). For the five animals with micro-hemorrhages also sonicated at 0.73 MPa, the average ΔSI was 21.3% ± 9.5%. The ΔSI ranged from 12.8% to 38.0% in three animals where 0.80 MPa sonications resulted in micro-hemorrhages and selective neuronal necrosis. In the other two animals sonicated at 0.80 MPa, ΔSI was 16.8% in the animal with multiple micro-hemorrhages and 71.5% in the animal with a hemorrhagic infarct. There was no clear

relationship between ΔSI and the presence and extent of the micro-hemorrhages (Table 4). In 9/15 animals, the sixth FUS session resulted in a lightly hyper-intense region on T2-WI in the sonicated area; in seven of these animals fresh micro-hemorrhages were observed.

Vascular damage produced during the previous FUS sessions—Table 3 provides an overview of the consequences of micro-vascular damage from the five earlier FUS sessions and effects observed on T2-WI. As tissue changes leading to hypo- or hyper-intensities on T2-WI probably resulted from micro-vascular damage during one of the previous sonications, ΔSI of the preceding session is provided in Table 3, as is the maximum ΔSI of all sessions per animal. Three animals without signs of a lesion on T2-WI had either a very small scar (0.2 × 0.3 mm), a small area with macrophage infiltration or showed no affected area at all. The maximum ΔSI ranged in these animals from 28.2% to 42.9%.

In four animals with a cyst formation, hyper-intense regions were present on T2-WI (Fig. 5). In all cases, the cyst resulted from micro-vascular damage probably produced during the first session, with ΔSI ranging from 24.9% to 58.1%. In two of these animals, mineralization spots were also present. These two animals also had hypo-intense spots on T2-WI.

In 7/15 animals, a hypo-intense spot on T2-WI was present for at least 2 wk. In 4/7 animals, the first or second session resulted in vascular damage, and in 3/7 animals small-vessel damage was produced during the third or fourth session. On the H&E sections, hemosiderin particles were found in all seven animals; four animals had a glial scar and mineralization spots were observed in three of them. The average ΔSI was 26.4% ± 10.0% on post-contrast T1-WI 1 wk before the hypo-intensity was observed.

For all five animals with mineralization spots, the hypo-intensity was observed on T2-weighted images for at least 4 wk. In 3/5 animals a persistent hyper-intensity was also observed on pre-contrast T1-WI. In one animal with a small scar, there was no evidence of a hypo-intensity, but an enlarged ventricle was observed on T2-WI.

DISCUSSION

In this study, MRI and histology were used to study the side effects of repeated BBB disruption using FUS in combination with micro-bubbles. Overall, it was demonstrated that the BBB can be disrupted repeatedly with limited or no significant effects evident in standard histology examinations. The results also suggest that without care to select an appropriate exposure level, tiny regions of vascular damage can result. BBB disruption was confirmed with contrast-enhanced T1-WI, but this technique had limited value for predicting the presence and extent of vascular damage. On the other hand, the observed tissue changes on histology corresponded well with T2-weigthed MRI, making this a valuable technique to follow the consequences of BBB disruption over time.

There are several mechanisms that have been suggested to be the basis for FUS-mediated BBB disruption in the presence of micro-bubbles. During the oscillating acoustic pressure, the micro-bubbles expand and shrink and the endothelial cells can be stimulated by processes like acoustic streaming, bubble oscillations and radiation force (Nyborg 2001). If the acoustic pressure is high enough, inertial cavitation can occur, leading to shock-waves or

jets. It has been shown that BBB disruption can be evoked without the presence of inertial cavitation (McDannold et al. 2006). In that same study, inertial cavitation has been associated with extravasations of erythrocytes, indicating that the micro-vessels have been ruptured, which can have heterogeneous consequences on the brain parenchyma. As the morphologic tissue changes take time to develop, the full extent of vessel damage can not immediately be observed on H&E sections.

The histologic effects observed here were consistent with what has been observed previously after a single session, suggesting that the process of repeatedly disrupting the BBB itself does not produce additional significant side effects. In many studies investigating the consequences of BBB disruption, histopathological sections were obtained after one sonication session (Baseri et al. 2010; Hynynen et al. 2005, 2006; McDannold et al. 2005). In some of these studies, fresh micro-hemorrhages were observed shortly after sonication; at later times, macrophages containing hemosiderin were observed. In the present study, the consequences of micro-vascular damage were observed at different stages of breakdown and repair. The signs of fresh and/or old micro-hemorrhages were present. Although not all animals were sacrificed immediately after the last sonication, micro-hemorrhages evoked by a sonication 36 h before the sacrifice were still recognizable by extravasated erythrocytes on the H&E sections. In some cases, mineral deposits, scar formations and micro-infarction sites were observed. However, in 4/15 animals no clinically significant side effects were detected after disruption of the BBB during six sessions. While all but one session led to successful BBB disruption, in 2/15 animals no signs of fresh or old hemorrhages were observed. The histologic effects of repeated stress to the brain vasculature were not systematically studied before. In a previous study, histologic and MRI data were obtained in one non-human primate after multiple sonications (McDannold et al. 2012). The authors reported similar effects: macrophage accumulation and scattered hemosiderin deposits at some targets, which corresponded with persistent hypo-intense spots in T2-weighted imaging during a follow-up period of 6 mo. In most locations, however, no effects were observed. Two studies have found no functional changes after repeated BBB disruption sessions in non-human primates (Downs et al. 2015; McDannold et al. 2012). Multiple sessions of BBB disruption have been shown to improve cognition in Alzheimer's model mice without evidence of damage (Burgess et al. 2014).

There was a positive relationship between the acoustic pressure and ΔSI, which corresponds to earlier results in rabbits (McDannold et al. 2006; O'Reilly and Hynynen 2012). However, there was no relationship between ΔSI and the presence of fresh hemorrhages produced during the last session. There was substantial overlap between the maximum ΔSI in animals without any significant effects and ΔSI leading to the formation of cysts or scars in other animals, so ΔSI had limited value for predicting the presence and extent of vascular damage. The animals sonicated at the highest pressure (group 3) had, in general, the largest affected areas and included the two animals with the most extensive damage. The least serious effects were observed in the lowest pressure group (group 1), although in one animal a small infarction had resulted in a small cyst.

The lowest acoustical pressure in water used here was 0.66 MPa. Assuming an attenuation of 33% by the rat skull at the used frequency (O'Reilly et al. 2011) and a attenuation of 0.05

Np/MHz at 1 cm in the brain, the estimated *in vivo* pressure was 0.43 MPa. This acoustic pressure corresponds to a mechanical index of 0.52, which is very close to the threshold (disruption probability of 50%) for BBB disruption in mechanical index of 0.46 (McDannold et al. 2008). The used pressures are thus in line with previously reported values for BBB disruption and the lowest pressures can be used as a directive for future research as the observed side effects were in general smallest for the lowest pressure group.

In this study, contrast-enhanced T1-WI was thus primarily of value in confirmation of BBB disruption. T2-WI corresponded well with the permanent effects observed on histopathology and can be used to adjust the acoustic pressure during the next treatment, to prevent small-vessel damage. In almost all animals with hemosiderin particles or mineralization present, a hypo-intense region was observed on T2-WI. However, we could not tell from these hypo-intensities whether a scar, mineralization or only hemosiderin particles were present. It has been reported that calcium deposits reduce both T1 and T2 relaxation times, leading to hyper-intensities on T1-WI and hypo-intensities on T2-WI (Dell et al. 1988). Selective neuronal necrosis and gliosis have the same MRI pattern (Fujioka et al. 1999). In three of five animals with mineralization spots, hyper-intensities on T1-WI have been observed. In the other two animals, no hyper-intensity on T1-WI was present or observed only during 1 wk. Hyper-intense regions on T2-WI were consistent with cyst formation and, probably, with liquefaction necrosis.

After most of the sonications, a light hyper-intense region on T2-WI was also observed. These hyper-intense regions were temporary and could indicate several effects. First of all, an acute hemorrhage might appear bright on T2-WI, due to the higher water content. This applies also for edema. As the T2-WI were obtained after contrast administration, these hyper-intensities could also be the effects of gadolinium, as our T2-weighted sequence had some T1-weighting in it due to the relatively short repetition time (2000 ms). We did not obtain T2*-weighted MRI, which would have made it possible to visualize fresh hemorrhages. Fresh hemorrhages appear as hypo-intensities on T2*-weighted (gradient-echo sequence) MRI due to the paramagnetic deoxyhemoglobin in the extravasated red blood cells (Hynynen et al. 2001). T2*-weighted MRI can also provide information about hemosiderin and calcifications, and the phase images of a gradient-echo sequence could be used to distinguish between the two (Gupta et al. 2001). Gradient-echo imaging could potentially provide even more information about the development of lesions after BBB disruption than T2-WI.

Our study had some limitations. First of all, the drawing of the ROIs to determine ΔSI was subjective, as was inspection of T2-WI and T1-WI for hyper- and hypo-intensities. The MRI voxels were relatively large (0.3 × 0.3 × 1 mm) compared to the microscopic tissue changes, which might have led to partial volume effects, limiting the detectability of effects on MRI. Although it was possible to disrupt the BBB repeatedly without clinically significant side effects, sometimes small glial scars (<0.5 mm) were present. The size of these scars was much smaller than the area with enhancement on T1-weighted imaging, which was >4.0 mm^2. If this technique would be used for tumor treatment, the expected benefit might outweigh these small side effects; however, vessel damage should be prevented, especially if used for less severe neurologic disorders. This outcome advocates for the use of a cavitation

detector to ensure that acoustic pressures below the inertial cavitation threshold can be used, as inertial cavitation has been associated with micro-hemorrhages (McDannold et al. 2006).

We demonstrated that it is possible to disrupt the BBB repeatedly with no or limited clinically significant side effects. In general side effects were small, but could be further limited by implementation of a cavitation detector to prevent inertial cavitation occurrence. The effects are consistent with prior studies that examined histologic effects after a single session. MRI gave valuable information about the success of the treatment and could be used to follow the effects of the treatments over time.

Acknowledgments

This study was financially supported by NIH grant P01 CA174645, ERC grant PIOF-GA-2012-331813, and Dutch Cancer Society (KWF 2013-5861), and a grant from CIMIT.

References

Abbott NJ, Romero IA. Transporting therapeutics across the blood-brain barrier. Mol Med Today. 1996; 2:106–113. [PubMed: 8796867]

Baseri B, Choi JJ, Tung Y-S, Konofagou EE. Multi-modality safety assessment of blood-brain barrier opening using focused ultrasound and definity microbubbles: a short-term study. Ultrasound Med Biol. 2010; 36:1445–1459. [PubMed: 20800172]

Bobo RH, Laske DW, Akbasak A, Morrison PF, Dedrick RL, Oldfield EH. Convection-enhanced delivery of macromolecules in the brain. Proc Natl Acad Sci. 1994; 91:2076–2080. [PubMed: 8134351]

Burgess A, Dubey S, Yeung S, Hough O, Eterman N, Aubert I, Hynynen K. Alzheimer disease in a mouse model: MR imaging–guided focused ultrasound targeted to the hippocampus opens the blood-brain barrier and improves pathologic abnormalities and behavior. Radiology. 2014; 273:736–745. [PubMed: 25222068]

Dell LA, Brown MS, Orrison WW, Eckel CG, Matwiyoff NA. Physiologic intracranial calcification with hyperintensity on MR imaging: case report and experimental model. AJNR Am J Neuroradiol. 1988; 9:1145–1148. [PubMed: 3143236]

Doolittle ND, Miner ME, Hall WA, Siegal T, Hanson EJ, Osztie E, McAllister LD, Bubalo JS, Kraemer DF, Fortin D, Nixon R, Muldoon LL, Neuwelt EA. Safety and efficacy of a multicenter study using intraarterial chemotherapy in conjunction with osmotic opening of the blood-brain barrier for the treatment of patients with malignant brain tumors. Cancer. 2000; 88:637–647. [PubMed: 10649259]

Downs ME, Buch A, Sierra C, Karakatsani ME, Chen S, Konofagou EE, Ferrera VP. Long-term safety of repeated blood-brain barrier opening via focused ultrasound with microbubbles in non-human primates performing a cognitive task. PLoS ONE. 2015; 10:e0125911. [PubMed: 25945493]

Fan L, Liu Y, Ying H, Xue Y, Zhang Z, Wang P, Liu L, Zhang H. Increasing of blood-tumor barrier permeability through paracellular pathway by low-frequency ultrasound irradiation in vitro. J Mol Neurosci. 2011; 43:541–548. [PubMed: 21104456]

Fujioka M, Taoka T, Matsuo Y, Hiramatsu K-I, Sakaki T. Novel brain ischemic change on MRI delayed ischemic hyperintensity on T1-weighted images and selective neuronal death in the caudoputamen of rats after brief focal ischemia. Stroke. 1999; 30:1043–1046. [PubMed: 10229742]

Guerin C, Olivi A, Weingart JD, Lawson HC, Brem H. Recent advances in brain tumor therapy: local intracerebral drug delivery by polymers. Invest New Drugs. 2004; 22:27–37. [PubMed: 14707492]

Gupta RK, Rao SB, Jain R, Pal L, Kumar R, Venkatesh SK, Rathore RK. Differentiation of calcification from chronic hemorrhage with corrected gradient echo phase imaging. J Comput Assist Tomogr. 2001; 25:698–704. [PubMed: 11584228]

Hynynen K, McDannold N, Sheikov NA, Jolesz FA, Vykhodtseva N. Local and reversible blood–brain barrier disruption by noninvasive focused ultrasound at frequencies suitable for trans-skull sonications. Neuroimage. 2005; 24:12–20. [PubMed: 15588592]

Hynynen K, McDannold N, Vykhodtseva N, Jolesz FA. Noninvasive MR Imaging–guided focal opening of the blood-brain barrier in rabbits. Radiology. 2001; 220:640–646. [PubMed: 11526261]

Hynynen K, McDannold N, Vykhodtseva N, Raymond S, Weissleder R, Jolesz FA, Sheikov N. Focal disruption of the blood–brain barrier due to 260-kHz ultrasound bursts: a method for molecular imaging and targeted drug delivery. J Neurosurg. 2006; 105:445–454. [PubMed: 16961141]

McDannold N, Arvanitis CD, Vykhodtseva N, Livingstone MS. Temporary disruption of the blood–brain barrier by use of ultrasound and microbubbles: safety and efficacy evaluation in rhesus macaques. Cancer Res. 2012; 72:3652–3663. [PubMed: 22552291]

McDannold N, Vykhodtseva N, Hynynen K. Blood-brain barrier disruption induced by focused ultrasound and circulating preformed microbubbles appears to be characterized by the mechanical index. Ultrasound Med Biol. 2008; 34:834–840. [PubMed: 18207311]

McDannold N, Vykhodtseva N, Hynynen K. Targeted disruption of the blood–brain barrier with focused ultrasound: association with cavitation activity. Phys Med Biol. 2006; 51:793. [PubMed: 16467579]

McDannold N, Vykhodtseva N, Raymond S, Jolesz FA, Hynynen K. MRI-guided targeted blood-brain barrier disruption with focused ultrasound: histological findings in rabbits. Ultrasound Med Biol. 2005; 31:1527–1537. [PubMed: 16286030]

Nyborg WL. Biological effects of ultrasound: Development of safety guidelines. Part II: General review. Ultrasound Med Biol. 2001; 27:301–333. [PubMed: 11369117]

O'Reilly MA, Hynynen K. Blood-Brain barrier: real-time feedback-controlled focused ultrasound disruption by using an acoustic emissions–based controller. Radiology. 2012; 263:96–106. [PubMed: 22332065]

O'Reilly MA, Muller A, Hynynen K. Ultrasound insertion loss of rat parietal bone appears to be proportional to animal mass at submega-hertz frequencies. Ultrasound Med Biol. 2011; 37:1930–1937. [PubMed: 21925788]

Pardridge WM. Drug and gene targeting to the brain with molecular trojan horses. Nat Rev Drug Discov. 2002a; 1:131–139. [PubMed: 12120094]

Pardridge WM. Drug and gene delivery to the brain: the vascular route. Neuron. 2002b; 36:555–558. [PubMed: 12441045]

Pardridge WM. Blood-brain barrier drug targeting: The future of brain drug development. Mol Interv. 2003; 3:90–105. [PubMed: 14993430]

Shang X, Wang P, Liu Y, Zhang Z, Xue Y. Mechanism of low-frequency ultrasound in opening blood–tumor barrier by tight junction. J Mol Neurosci. 2011; 43:364–369. [PubMed: 20852968]

Sheikov N, McDannold N, Jolesz F, Zhang Y-Z, Tam K, Hynynen K. Brain arterioles show more active vesicular transport of blood-borne tracer molecules than capillaries and venules after focused ultrasound-evoked opening of the blood-brain barrier. Ultrasound Med Biol. 2006; 32:1399–1409. [PubMed: 16965980]

Sheikov N, McDannold N, Sharma S, Hynynen K. Effect of focused ultrasound applied with an ultrasound contrast agent on the tight junctional integrity of the brain microvascular endothelium. Ultrasound Med Biol. 2008; 34:1093–1104. [PubMed: 18378064]

Xia C, Liu Y, Wang P, Xue Y. Low-frequency ultrasound irradiation increases blood–tumor barrier permeability by transcellular pathway in a rat glioma model. J Mol Neurosci. 2012; 48:281–290. [PubMed: 22528460]

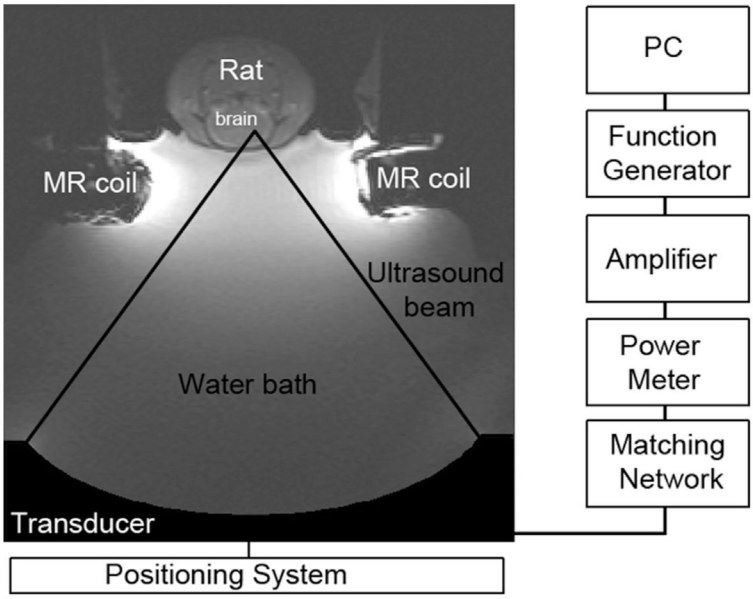

Fig. 1.

The setup for the focused ultrasound treatments. The rat was placed in supine position in a holder on top of a water bath. The 690-kHz transducer was placed in the water bath and connected to a positioning system and matching network. To obtain the magnetic resonance images, a home-made transmit/receive surface coil was used.

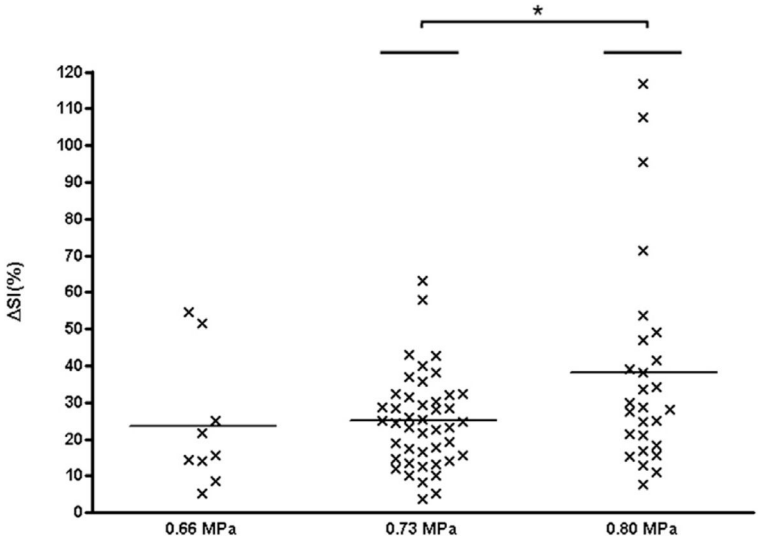

Fig. 2.

Signal enhancement versus acoustic pressure. For each session, the difference in signal intensity change between the treated and untreated (contralateral) brain regions in pre- and post-sonication contrast-enhanced T1-WI (ΔSI) is plotted against the used acoustic pressure. The horizontal bars indicate the mean and the asterisk a significance difference of $p < 0.05$.

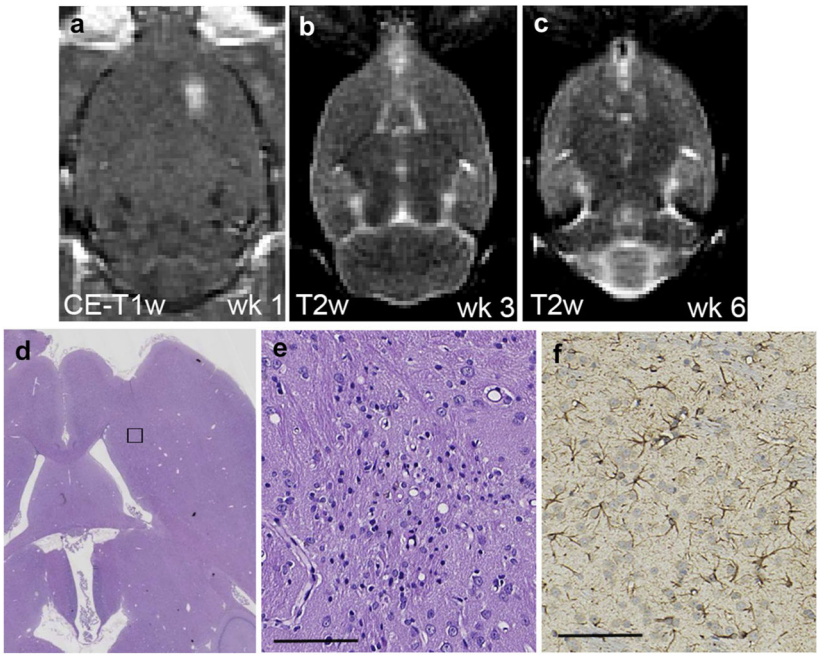

Fig. 3.

Representative magnetic resonance images and histology of an animal with a micro-scar after six successful blood–brain barrier disruption sessions. (a) Axial contrast-enhanced T1-WI showing blood–brain barrier disruption after the first session (ΔSI = 21.8%). An acoustic pressure of 0.66 MPa was used for the first three sessions and 0.73 MPa for the following three sessions. (b and c) No abnormalities were observed during the following weeks on axial T2-weighted imaging. (d) A micro-scar (0.2 × 0.3 mm) and small area with macrophage infiltration was observed on the hematoxylin & eosin (H&E) section. (e) Higher magnification of the affected area shown in rectangular in (d). (f) At the same location, glial fibrillary acidic protein (GFAP)-immunolabeled astrocytes are identified as being reactive based on their thick cytoskeletal processes (d and e: H&E, f: GFAP). Scale bars: 0.1 mm.

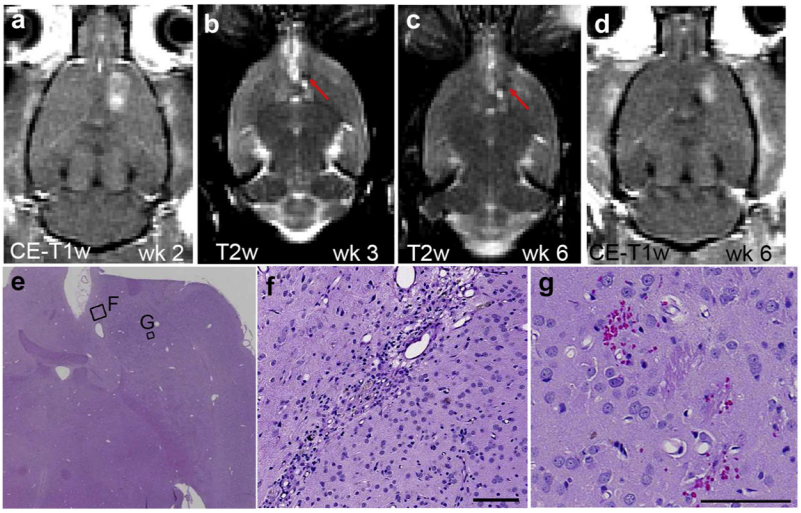

Fig. 4.

Representative magnetic resonance images and histology of an animal with a hypointense lesion on T2-weighted imaging (T2-WI). (a) Contrast-enhanced T1-WI showing blood–brain barrier (BBB) disruption after the second session (ΔSI = 14.2%). BBB disruption was successful for each session using an acoustic pressure of 0.73 MPa. (b and c) In the following weeks a hypo-intense spot was observed on T2-WI (red arrows). Note the hyper-intensity adjacent to the hypo-intense spot is the ventricle. (d) Contrast-enhanced T1-WI showing BBB disruption after the sixth session (ΔSI =15.7%). (e) On the hematoxylin & eosin (H&E) section, two separate areas were present with different histopathological features, presumably the result of the sonication in different sessions, with higher magnifications shown in (f) and (g). (f) The affected area includes a small (1.8 × 0.2 mm) scar and a few hemosiderin particles. (g) Affected area that shows a few scattered petechiae probably produced during the last BBB disruption session (e–g: H&E). Scale bars: 0.1 mm.

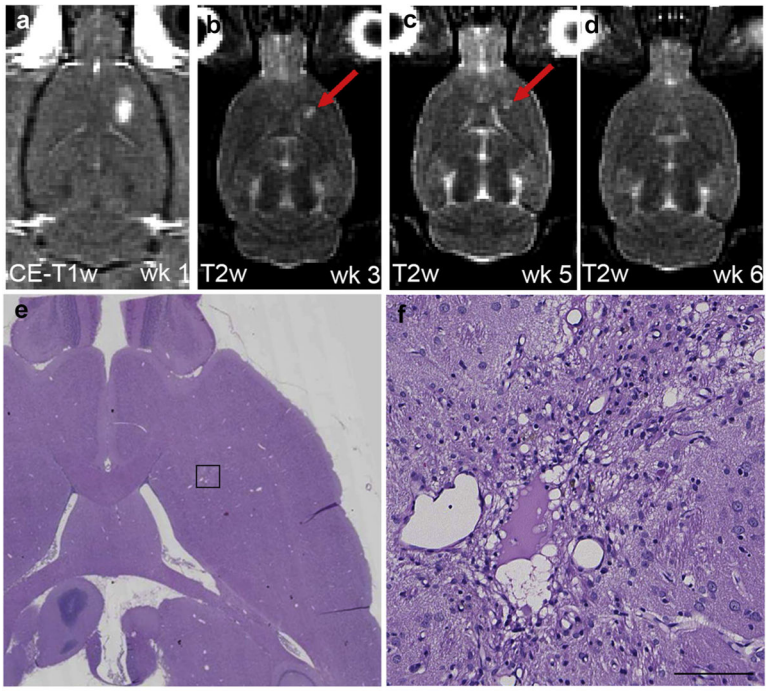

Fig. 5.

Magnetic resonance imaging and histology of an animal that developed a cyst after the first sonication. (a) Axial contrast-enhanced T1-weighted imaging (T1-WI) showed blood–brain barrier (BBB) disruption after the first session (ΔSI = 51.6%). The animal was sonicated at 0.66 MPa during the first three sessions and 0.73 MPa for the next three sessions. (b–d) In pre-sonication T2-WI, a hyper-intense area (*red arrow*) was observed during the following weeks, decreasing over time and no longer apparent at week 6. (e and f) An affected area (~2.0 × 1.5 mm) with scar formation and residuals of a cyst suggests a previous micro-infarct. The lateral ventricle appeared slightly enlarged. (f) Higher magnification of the affected area shown in rectangular in (e) (e and f: H&E). Scale bar: 0.1 mm.

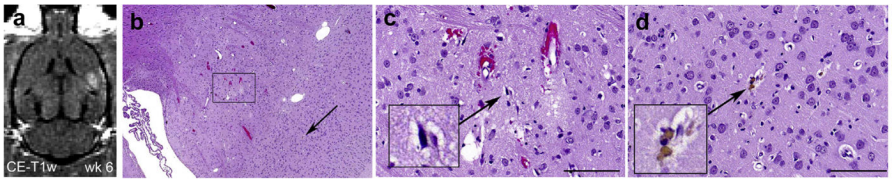

Fig. 6.

T1-weighted imaging from the last focused ultrasound session that resulted in micro-hemorrhages and selective neuronal necrosis as observed on histology. (a) Contrast-enhanced T1-weighted imaging shows successful blood–brain barrier disruption (ΔSI = 15.6%) when sonicated at 0.80 MPa. (b) In the treated area, small-vessel damage occurred, which is characterized by extravasations of erythrocytes and selective neuronal necrosis. (c) Higher magnification of the affected area (rectangular in [b]) showing individual dark, shrunken (ischemic) neurons (inset) and a slightly vacuolated neuropil. (d) A single hemosiderin particle (inset, arrow in [b]) signifies an old micro-hemorrhage in the intact neuropil (b–d: H&E). Scale bars: 0.1 mm.

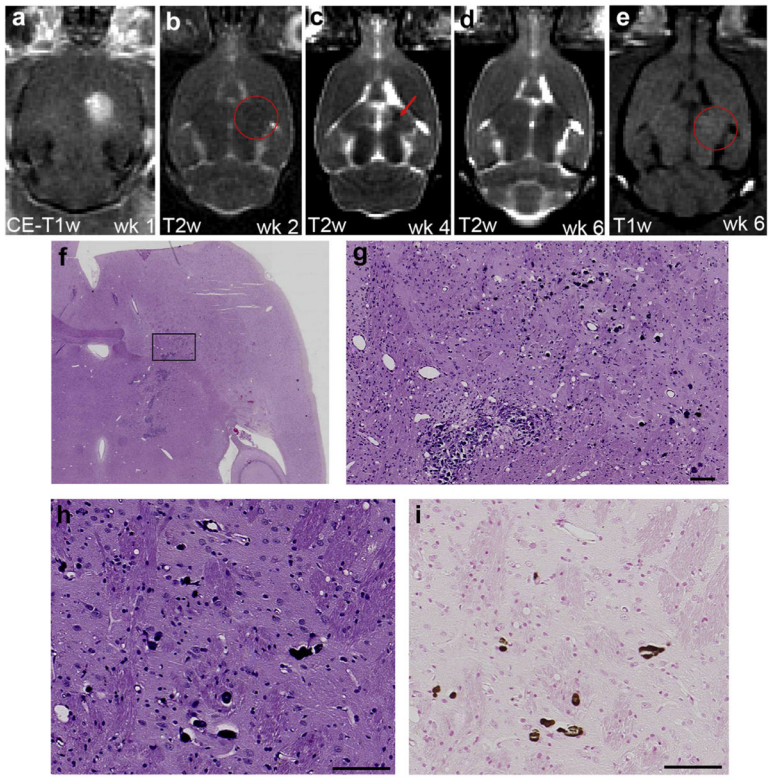

Fig. 7.

Magnetic resonance images and histopathological data of an animal with multifocal mineralization deposits. (a) Contrast-enhanced T1-weighted imaging (T1-WI) showed successful blood–brain barrier disruption after the first session (ΔSI = 34.2%) when sonicated at 0.80 MPa. (b) One week later, a diffuse hypo-intense area (red circle) was visible on post-sonication T2-WI. (c and d) Post-sonication T2-WI showed a focal hypo-intense region (*red arrow*) during the following weeks. (e) During these weeks, a hyper-intense region (red circle) was also present on pre-sonication T1-WI, which might indicate the presence of calcium deposits. (f) Large affected region including multifocal deposits of mineralization in the thalamus and putamen. (g) Higher magnification of the affected area (rectangular in [f]) with microscopic mineralization in the sites of former neuronal necrosis. (h and i) Mineralization spots under the highest magnification on hematoxylin & eosin (H&E) (h) and Von Kosssa staining (i) (f–h: H&E; i: Von Kossa). Scale bars: 0.1 mm.

Table 1

Magnetic resonance imaging parameters

MR sequence	Echo time (ms)	Repetition time (ms)	Slice thickness (mm)	Field of view (cm)	Matrix	Number of signal averages	Echo train length
T1-weighted imaging	13	500	1.5	8 × 8	256 × 256	4	4
T2-weighted imaging	91	2000	1.5	8 × 8	256 × 256	2	8

Table 2

Characteristics of the three treatment groups

		Acoustic pressure (MPa)						
Animal ID	**Weight week 1, g mean (range)**	**week 1**	**week 2**	**week 3**	**week 4**	**week 5**	**week 6**	**Sacrifice after the last session**
1–5	325 (309–339)	0.66	0.66	0.66	0.73	0.73	0.73	~24 h
6–10	277 (224–353)	0.73	0.73	0.73	0.73	0.73	0.73	~22–36 h
11–15	197 (155–346)	0.66 (n = 1) 0.73 (n = 1) 0.80 (n = 3)	0.80	0.80	0.80	0.80	0.80	<3.5 h

Table 3

Overview of the permanent effects from the sonications as seen on histology and magnetic resonance imaging

		Histopathology					MRI						
			Affected area contains:				T2-WI		T1-WI	Contrast-enhanced T1-WI		
Animal ID	Acoustic pressure, MPa	Size glial scar (mm)	Macrophages	Hemosiderin	Mineralization	Cystic cavity	Permanent effects on T2-WI	Wk with permanent effect on T2-WI	Wk with permanent hyper-intensity on pre-contrast T1-WI	ΔSI one wk before permanent effects on T2-WI (wk)	Maximum ΔSI (wk)	Note:
1	0.66 & 0.73	0.2 × 0.3	+	+	−	−	Hypo-intensity	Wk: 5–6		28.4 (wk 4)	54.5 (wk 1)	NA (wk 2)
2	0.66 & 0.73	0.2 × 0.3	+	−	−	−	-	-		-	28.2 (wk 4)	NA (wk 2)
3	0.66 & 0.73	0.3 × 0.7	+	+	−	+	Hyper-intensity	Wk: 3–5		51.6 (wk 1)	51.6 (wk 1)	NA (wk 2)
4	0.66 & 0.73	0.2 × 0.3	+	−	−	−	Enlarged ventricle	Wk: 3–6		NA: wk 1/2 (wks 1 & 2)	32.5 (wk 5)	NA (wk 1 & 2)
5	0.66 & 0.73	0	−	−	−	−	-	-		-	28.7 (wk 6)	NA (wk 1 & 2)
6	0.73	>0.5 × 0.7	+	+	+	+	Hyper-intensity Hypo-intensity	Wk: 2–6 Wk: 3–6		24.9 (wk 1) 40.0 (wk 2)	40.0 (wk 2)	
7	0.73	0.2 × 0.2	+	+	+	−	Hypo-intensity	Wk: 3–6		23.4 (wk 2)	35.8 (wk 1)	
8	0.73	0.2 × 0.8	+	+	+	−	Hypo-intensity	Wk: 3–6	Wk: 2–6	14.2 * (wk 2)	25.4 (wk 3)	
9	0.73	0	+	−	−	−	-	-		-	42.7 & 42.9 (wks 1 & 6)	
10	0.73	1.6 × 0.9	+	+	−	+	Hyper-intensity	Wk: 2–6	Wk: 3–6	58.1 (wk 1)	63.1 (wk 2)	
11	0.80	1.4 × 4.0	+	+	+	−	Hypo-intensity Enlarged ventricle	Wk: 2–6 Wk 2–6	Wk: 2–6	34.2 (wk 1)	49.0 (wk 3)	
12	0.66 & 0.80	0	+	+	−	−	Hypo-intensity	Wk: 2–5		14.3 † (wk 1)	46.9 (wk 2)	NA (wk 6)
13	0.73 & 0.80	0	+	+	−	−	Hypo-intensity	Wk: 5–6		28.7 (wk 4)	28.7 (wk 4)	
14	0.80	0	+	+	−	−	Hypo-intensity	Wk: 4–6		41.5 (wk 3)	41.5 (wk 3)	
15	0.80	3.7 × 2.7 + 3smaller spots <0.4 × 0.4	+	+	+	+	Hyper-intensity Enlarged ventricle Hypo-intensity	Wk: 2–6 Wk: 2–6 Wk: 4–6	Wk: 3–6	39.1 (wk 1) 107.6 (wk 3)	116.9 (wk 5)	

MRI = magnetic resonance imaging; T2-WI = T2-weighted imaging; T1-WI = T1-weighted imaging; NA = data not available.

* For week 1 and 2, only one pre-contrast T1-weighted slice was available; however, this was not the slice with the most prominent contrast enhancement. The difference between the enhancing region and the contralateral region in the plane with the most-enhancing area gave a difference of 48% for week 1 and 46% for week 2.

† The location of the hypo-intense region corresponds better with the strong enhancement of week 2, than the weaker enhancement of week 1, which was a bit more anterior.

Table 4

Effects observed on histopathology and magnetic resonance imaging of the sixth blood–brain barrier disruption session

				MRI	
Animal ID	**Weight week 6, g**	**Acoustic pressure, MPa**	**Histopathology**	**ΔSI (%)**	**T2-WI**
1	455	0.73	No effects	37.1	Light hyper-intensity
2	426	0.73	No effects	13.1	-
3	362	0.73	A few tiny micro-hemorrhages	31.5	Light hyper-intensity
4	370	0.73	A few tiny micro-hemorrhages	22.7	Light hyper-intensity
5	425	0.73	Micro-hemorrhages	28.7	Light hyper-intensity
6	430	0.73	Micro-hemorrhages	8.2	-
7	420	0.73	No effects	5.3	-
8	400	0.73	A few tiny micro-hemorrhages	15.7	Light hyper-intensity
9	490	0.73	No effects	42.9	Light hyper-intensity
10	470	0.73	No effects	17.6	-
11	374	0.80	Micro-hemorrhages + selective neuronal necrosis	38.0	-
12	389	0.80	Micro-hemorrhages + selective neuronal necrosis	15.6	NA*
13	401	0.80	Multiple extensive micro-hemorrhages	16.8	Light hyper-intensity
14	398	0.80	Micro-hemorrhages + selective neuronal necrosis	12.8	Light hyper-intensity
15	473	0.80	Hemorrhagic infarct	71.5	Light hyper-intensity

MRI = magnetic resonance imaging; ΔSI = difference in signal intensity change in pre- and post-sonication T1-WI.

*NA = data not available.